Biosensors and Bioelectronics 133 (2019) 192–198

Contents lists available at ScienceDirect

Biosensors and Bioelectronics

journal homepage: www.elsevier.com/locate/bios

Quench-type electrochemiluminescence immunosensor for detection of amyloid β-protein based on resonance energy transfer from luminol@SnS_2-Pd to Cu doped WO_3 nanoparticles

Jingwei Xue[a], Lei Yang[a], Huan Wang[a,*], Tao Yan[b], Dawei Fan[a], Rui Feng[b], Bin Du[a,b], Qin Wei[a,*], Huangxian Ju[a,c]

[a] Key Laboratory of Interfacial Reaction & Sensing Analysis in Universities of Shandong, School of Chemistry and Chemical Engineering, University of Jinan, Jinan 250022, PR China
[b] School of Water Conservancy and Environment, University of Jinan, Jinan 250022, PR China
[c] Key Laboratory of Analytical Chemistry for Life Science, School of Chemistry and Chemical Engineering, Nanjing University, Nanjing 210023, PR China

ARTICLE INFO

Keywords:
Copper doped tungsten trioxide
Electrochemiluminescence
Luminol
Resonance energy transfer
Amyloid β-protein

ABSTRACT

A highly efficient quench-type electrochemiluminescence (ECL) immunosensor was proposed for the trace detection of amyloid β-protein ($A\beta_{1-42}$). In this work, tin disulfide nanoflowers (SnS_2 NFs) with large specific surface area, favorable catalytic property and chemical stability were prepared and used as substrate material. Taking advantage of the excellent catalytic ability and biocompatibility, palladium nanoparticles (Pd NPs) were in situ reduced on SnS_2 NFs to obtain SnS_2-Pd. Moreover it could combine with large amounts of luminol and achieve a strong ECL signal output. In addition, copper doped mesoporous tungsten trioxide (Cu:WO_3) nanoparticles were selected to quench ECL emission of luminol@SnS_2-Pd via resonance energy transfer, where luminol@SnS_2-Pd was the donor and Cu:WO_3 was the acceptor. On this basis, a quench-type ECL immunosensor was constructed for detection of $A\beta_{1-42}$. Under optimum conditions, the fabricated ECL immunosensor showed sensitive response to $A\beta_{1-42}$ concentration from 0.1 pg/mL to 50 ng/mL with a low detection limit of 5.4 fg/mL (S/N = 3). It is expected to be a promising analytical tool for the sensitive detection of $A\beta_{1-42}$ and other biomarkers with high specificity, good reproducibility and long-term stability.

1. Introduction

In the past decade, various electrochemiluminescence sensors (Ahmed et al., 2014; Jia et al., 2019; Jin et al., 2016; Yang et al., 2017b) have been proposed for analyzing biomarkers of human serious diseases like cancers (Kadimisetty et al., 2015), Parkinson's disease and Alzheimer's disease in clinical diagnosis, which has greatly contributed to the advances in precision and personalized medicine. Among these diseases, Alzheimer's disease (AD) is a neurological disease whose specific pathogenesis is still in an uncertain state (Ren et al. 2017c; Sloan et al., 2012). Patients with AD would experience symptoms of diminished memory, slowness, and poor cognitive ability or even disappearance, which seriously affected patients' lives (Sperling et al., 2011). Thus, realizing the early diagnosis of AD is particularly important. Due to the fact that amyloid β-protein ($A\beta_{1-42}$) oligomers was closely related to the pathogenesis of AD because of its extremely strong neurotoxicity, the early diagnosis of $A\beta_{1-42}$ oligomers in human cerebrospinal fluid (CSF) is of great significance for early prevention and treatment for AD.

With superiority of high sensitivity, strong specificity, low background signal and wide response linear range, electrochemiluminescence (ECL) immnunoassay has been widely developed in biochemical analysis (Rizwan et al., 2018; Yang et al., 2017a), clinical diagnostics (Huang et al., 2017; Ma et al., 2017) and environmental pollutant monitoring (Afsharmohajer et al., 2018). Hydrogen peroxide (H_2O_2)-luminol system was one of the most widely used ECL strategy (Cao et al., 2012). Combining luminol with nanostructured enzyme mimic nanomaterials could greatly facilitate the ECL process since H_2O_2 was efficiently catalyzed to produce reactive oxygen species (ROSs) including $OH^{\bullet}$ and $O_2^{\bullet -}$, thus promoting the ECL emission of luminol to get strong ECL signals.

To date, nanostructured enzyme mimics have been widely used in luminol-based ECL immnunoassay on account of their excellent catalytic property and good stability (Ahmed and Lim, 2016; Long et al.,

* Corresponding authors.
E-mail addresses: chm_wanghuan@ujn.edu.cn (H. Wang), chm_weiq@ujn.edu.cn (Q. Wei).

https://doi.org/10.1016/j.bios.2019.03.035
Received 14 January 2019; Received in revised form 16 March 2019; Accepted 18 March 2019
Available online 19 March 2019
0956-5663/

2018; Ren et al., 2017a; Zhang et al., 2018). Based on previous work, sulfide has been extensively studied in electrochemistry because it can catalyze the decomposition of H_2O_2 to produce large amounts of ROSs (Chianelli et al., 1994; Ren et al. 2017b; Xiang et al., 2018). Recently, tin disulfide (SnS_2), as a qualified H_2O_2 catalyzer, has been extensively used in many fields such as electrochemistry (Chang et al., 2012; Jin et al., 2018; Warczak et al., 2018), battery (Ahmed et al., 2016; Liu and Crooks, 2012; Zhou et al., 2014) and photocatalysis (Deng et al., 2017; Shi et al., 2017) because of favorable electronic, optical and physicochemical properties. However, catalytic ability of pure SnS_2 are limit, thus composite materials are taken into account. Noble metals have been confirmed as excellent catalytic materials (Hu et al., 2018; Yang et al., 2017c), especially palladium nanoparticles (Pd NPs) were frequently used as catalyst for H_2O_2. Furthermore, SnS_2-Pd can combine with large amounts of luminol molecules via electrostatic adsorption. Therefore, SnS_2-Pd is expected to be a suitable material. Thanks to the dual catalyzing effect, luminol@SnS_2-Pd can exhibit stronger ECL signal than pure luminol, thus it is expected to be an excellent luminophor.

In order to modulate the ECL emission of luminol@SnS_2-Pd in an appropriate level to indicate the weak concentration changes of analytes so as to achieve a higher sensitivity, finding a quenching probe is necessary. Tungsten trioxide (WO_3) as a kind of n-type semiconductor material was found with favorable electronic, optical chemical properties (Lu et al., 2005) and good ultraviolet absorption ability. As is known to all, luminol can emit blue light with a wavelength of 425 nm in the ECL emission process, which shows a fine overlap with the UV-vis absorption spectrum of WO_3. What's more, copper doped tungsten trioxide (Cu:WO_3) can further increase the absorption peak area to achieve better result. Inspired by this, Cu:WO_3 was expected to be utilized to absorb the light generated by luminol@SnS_2-Pd via resonance energy transfer.

In view of above, a novel quench-type ECL immunosensor for $A\beta_{1-42}$ detection was developed utilizing luminol@SnS_2-Pd as energy donor and as energy acceptor. Luminol@SnS_2-Pd generated high and stable ECL signals in the presence of H_2O_2 and the primary antibody of $A\beta_{1-42}$ (Ab_1) which could be captured via Pd-N bond. Then, Cu:WO_3 was functionalized by gold nanoparticles (Au NPs) to capture the secondary antibody (Ab_2) via Au-N bond (Xing et al., 2018). When $A\beta_{1-42}$ was incubated to form the sandwich like immune-complex, the ECL emission of luminol@SnS_2-Pd was efficiently quenched by Cu:WO_3 via resonance energy transfer, thus realizing the sensitive detection of $A\beta_{1-42}$ in human CSF. With favorable stability, specificity and repeatability, this proposed quenching strategy surely provides a new prospective for sensitive analysis of $A\beta_{1-42}$ and other biomarkers and contributes to the developments of precision and personalized medicine in the future.

2. Experimental section

2.1. Reagents and apparatus

The amyloid β-protein oligomers ($A\beta_{1-42}$) and their antibodies (Ab_1, Ab_2) were obtained from Huaan Magnech Bio-Tech Co., Ltd. (Beijing, China). The other reagents and all of the apparatus are in Supplementary Material. The acquisition and use of human CSF sample was approved by the Institutional Ethics Committee of University of Jinan.

2.2. Preparation of luminol@SnS_2-Pd

First of all, 3D SnS_2 NFs were prepared by a previously reported hydrothermal method (Jing et al., 2017) with a slight modification, and the detailed process was shown in Supplementary material. 2 mg of SnS_2 NFs were dissolved in 1 mL deionized water, then 2 mL of 2% H_2PdCl_4 (60 mM) and 10 mg of PVP were added into the above solution. The mixture was kept stirring for 12 h at room temperature. After that, 10 mg of $NaBH_4$ and 14 mL of sodium citrate (150 mM) was added into mixture and maintained stirring for 12 h. After centrifugation and washing, the SnS_2-Pd composite was obtained. Then, 2 mg of luminol@SnS_2-Pd was dissolved into 2 mL of luminol (5 mM), and oscillated for 12 h. The supernatant was separated by centrifugation, luminol@SnS_2-Pd was obtained and dispersed into 1 mL of PBS (pH 7.4) and stored at 4 °C until use.

2.3. Preparation of mesoporous Cu:WO_3 nanoparticles

Firstly, sodium tungstate ($Na_2WO_4{\cdot}2H_2O$, 0.1 M), phthalic acid ($C_6H_8O_7$, 0.01 M) and copper acetate (CH_3COOCu, 0.02 M) were dissolved in 100 mL of deionized water. Then, the pH value of the prepared solution was adjusted to 1 by the addition of HNO_3 (1 M). After stirring for 3 h, the color of the solution changed to yellow, the tungstic acid was formed. The mixed solution was treated by ultrasonic for another 3 min and washed 3 times with anhydrous ethanol. In the end, the powder was sintered at 500 °C for 3 h, and Cu:WO_3 was obtained (Fu and Zhou, 2011). Meanwhile, the pure WO_3 nanoparticles were prepared without the addition of copper acetate.

2.4. Preparation of Cu:WO_3-Au-Ab_2

The gold nanoparticles (Au NPs) were synthesized according to Frens's method (Frens, 1973) and the detailed process was showed in Supplementary material. Cu:WO_3-Au-Ab_2 bioconjugate was synthesized according to previous report (Xiang et al., 2013) with a slight modification. First of all, 1 mL of Au NPs was added to 1 mL of Cu:WO_3 (2 mg/mL) solution and oscillated for 12 h. After centrifugation, Cu:WO_3-Au was dispersed into 1 mL of PBS (pH 7.4), then 100 μL of Ab_2 (10 μg/mL) was added into the above solution, and then incubated at 4 °C for 12 h. After centrifugation, the obtained solid was dissolved in 1 mL of PBS (pH 7.4) and stored at 4 °C until use (Feng et al., 2017).

2.5. Fabrication of the immunosensor for detecting $A\beta_{1-42}$

The glassy carbon electrode (GCE) (Φ = 4 mm) was polished to mirror surface by using alumina powder with different granularity (0.05 μm and 0.03 μm). The fabrication process of the proposed ECL immunosensor was shown in Scheme 1. First of all, the bare GCE was modified with 6 μL of luminol@SnS_2-Pd solution, and dried at room temperature. Then, 6 μL of Ab_1 (10 mg/mL) was incubated overnight (12 h) to obtain luminol@SnS_2-Pd-Ab_1. Next, 3 μL of BSA (1%) was modified on the electrode to block the non-specific active sites and then dried at room temperature. After that, the electrode was carefully washed with PBS (pH 7.4). Subsequently, a series of different concentrations of $A\beta_{1-42}$ were incubated and dried at 4 °C. Then, 6 μL of Cu:WO_3-Au-Ab_2 was modified on the electrode surface and dried at room temperature. Finally, the ECL immunosensor was constructed and stored at 4 °C for the following testing.

2.6. ECL measurements of immunosensor

In this experiment, a three-electrode system was used to test the immunosensor system, which Ag/AgCl as reference electrode, platinum electrode as counter electrode, and the electrode with different modification states as working electrode. To limit the consecutive reaction between luminol and H_2O_2 and be efficient to keep luminol ECL intensity, the single-step cycle pulse was applied in this work. The ECL measurement was performed in 10 mL of PBS (pH 7.8) containing 6 mM H_2O_2 with pulse potential at 0.7 V, pulse time at 0.3 s, initial potential at −0.3 V and pulse period at 7.5 s. The voltage of the photomultiplier tube (PMT) was set as 600 V to optimize substrate concentration, electrolyte, pH, concentration of co-reactant, and other experimental conditions which could affect the performance of the ECL immunosensor.

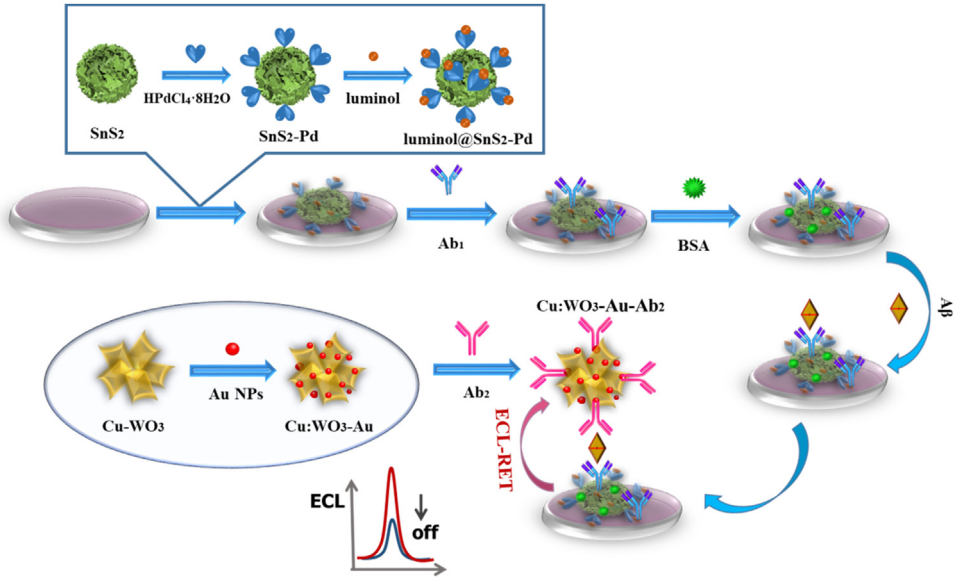

Schemee 1. Fabrication process of the proposed ECL immunosensor.

3. Results and discussions

3.1. Material characterization

Scanning electron microscope (SEM) and transmission electron microscope (TEM) were used to observe the morphologies of nanoparticles. X-ray diffraction (XRD) was utilized to reveal structural information and degree of crystallinity about the samples. Energy dispersive spectrometer (EDS) and transmission electron microscope mapping were used for elemental component analysis.

Pure SnS_2 NFs presented a flower-like structure with an average size of approximately 1.5 μm (Fig. S1A). TEM images were used to further determine the structure of SnS_2, a flower-shaped structure with multilayer nanoplates was clearly shown (Fig. 1A and B). This structure provided a large amount of binding sites to immobilize luminol and Pd NPs through in situ reduction. TEM mapping (inset of Fig. 1A) and EDS (Fig. S2A) of SnS_2 showed the existence of Sn and S elements. XRD (Fig. S1C) was used to characterize the crystallization of SnS_2. Specific sharp peaks of different planes were found at 15.029°, 28.199°, 32.124°, 46.121°, 52.451°, 54.960° and 62.968°, which corresponded to the (001), (100), (101), (003), (111), (103) and (004) planes of SnS_2 NFs, respectively (JCPDS Card NO. 39-0354). As shown in Fig. S1B, a large number of Pd NPs were distributed on the surface of SnS_2. Moreover, the success of in situ reduction of Pd NPs was proved by EDS energy spectrum (Fig. S2B).

As shown in Fig. S1D, it could be observed that Cu:WO_3 showed a mesoporous structure with an average size of 200 nm. This structure was further proved by TEM (Fig. 1C and D). Depending on TEM mapping (inset of Fig. 1C) and EDS spectrum (Fig. S2C), it showed the existence of Cu, W and O elements, indicating the successful doping of copper. XRD (Fig. S1E) was used to characterize the crystallization of Cu:WO_3. Several sharp peaks were found at 23.143°, 23.643°, 24.366°, 28.401°, 35.495°, 43.428°, 47.253°, and 55.403°, which corresponded the (002), (020), (200), (− 112), (122), (203), (004) and (-402) planes of WO_3 nanoparticles, respectively (JCPDS Card NO. 43-1035). Moreover, there was almost unchanged of the diffraction pattern between copper doped and undoped. It indicated that the doping of copper didn't cause the structural change of WO_3. Then, SEM image of Cu:WO_3-Au (Fig. S1F) showed lots of Au NPs were distributed on Cu:WO_3 uniformly, which was further confirmed by the EDS spectrum and UV-vis absorption spectra (Fig. S2D and Fig. S3). All of the results indicated the successful preparation of Cu:WO_3-Au.

3.2. Optimization of the experimental conditions

The influence curve of substrate concentration on ECL response of the immunosensor is shown in Fig. 2A. As the luminol@SnS_2-Pd concentration increased, the signal strength of the immunosensor also increased. When the luminol@SnS_2-Pd concentration was 2 mg/mL, the electroluminescent signal reached the maximum, and when the concentration exceeded 2 mg/mL, the ECL signal was decreased that was overfull substrate hindered electron transmission. Therefore, the experimental results showed that 2 mg/mL was the optimal concentration of the luminol@SnS_2-Pd. As shown in Fig. 2B, the ECL intensity showed an obvious increasing trend with the increase of concentration of H_2O_2. When the concentration was 6 mM, the ECL signal reached the maximum, and then reached a stable platform. The results showed that 6 mM was the optimal concentration of H_2O_2. As shown in Fig. 2C, when pH changed from 6.8 to 7.8, the ECL signal of the immunosensor showed an upward trend. When pH continued to increase from 7.8 to 8.8, the ECL signal showed a downward trend. Thus, the optimum pH value of 7.8 was selected. In addition, the concentrations of Cu:WO_3 for this immunosensor was also considered. As shown in Fig. 2D, the immunosensor was used for the detection of 0.1 ng/mL $A\beta_{1-42}$. As a result, the ECL intensity changed with the concentrations of Cu:WO_3. When the concentrations of Cu:WO_3 was 2.5 mg/mL, the ECL intensity between GCE/luminol@SnS_2-Pd-Ab_1 and GCE/luminol@SnS_2-Pd-Ab_1/BSA/$A\beta_{1-42}$/ Cu:WO_3-Au-Ab_2 reached a platform, thus 2.5 mg/mL Cu:WO_3 was chosen as the optimal concentration.

3.3. Mechanism investigation of luminol@SnS_2-Pd/H_2O_2 system

Referencing the previous studies, H_2O_2 is one efficient coreactant for luminol ECL emission, which could be decomposed to generate $O_2^{\bullet -}$ and $OH^{\bullet}$. Recently, more and more catalysts have been studied to catalyze the decomposition of H_2O_2 (Ghedini et al., 2010) with high efficiency. In this work, the dual catalytical property of SnS_2-Pd was applied to in the reduction of H_2O_2 which could generate more $O_2^{\bullet -}$ and $OH^{\bullet}$. Same amounts of luminol could reacted with more $O_2^{\bullet -}$ and $OH^{\bullet}$ per unit time, thus further the strong ECL signal output. To verify the dual catalytic property of SnS_2-Pd, the ECL behaviors of the bare GCE modified with luminol (curve a), luminol@SnS_2 (curve b), and luminol@SnS_2-Pd (curve c) were detected in PBS (pH 7.8) containing 6 mM H_2O_2. As shown in Fig. 3A, the ECL signal from curve a to curve c gradually increased.

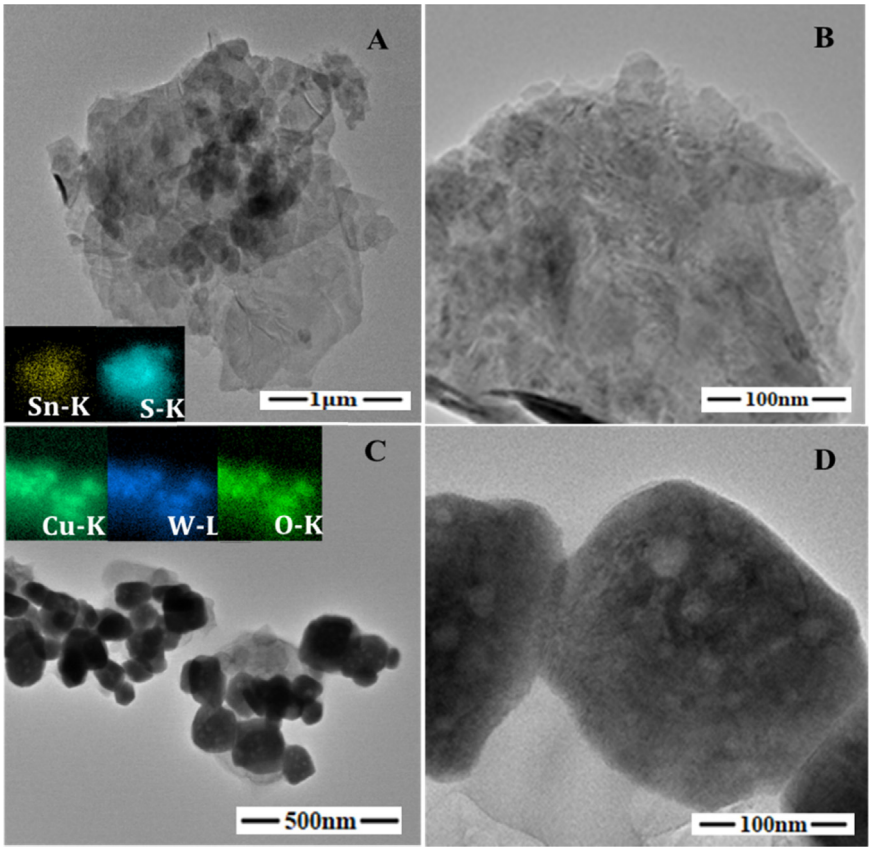

Fig. 1. TEM image of SnS_2 (A, B) and the TEM mapping of SnS_2 (inset of A), TEM image of Cu:WO_3 (C,D) and the TEM mapping of Cu:WO_3 (inset of C).

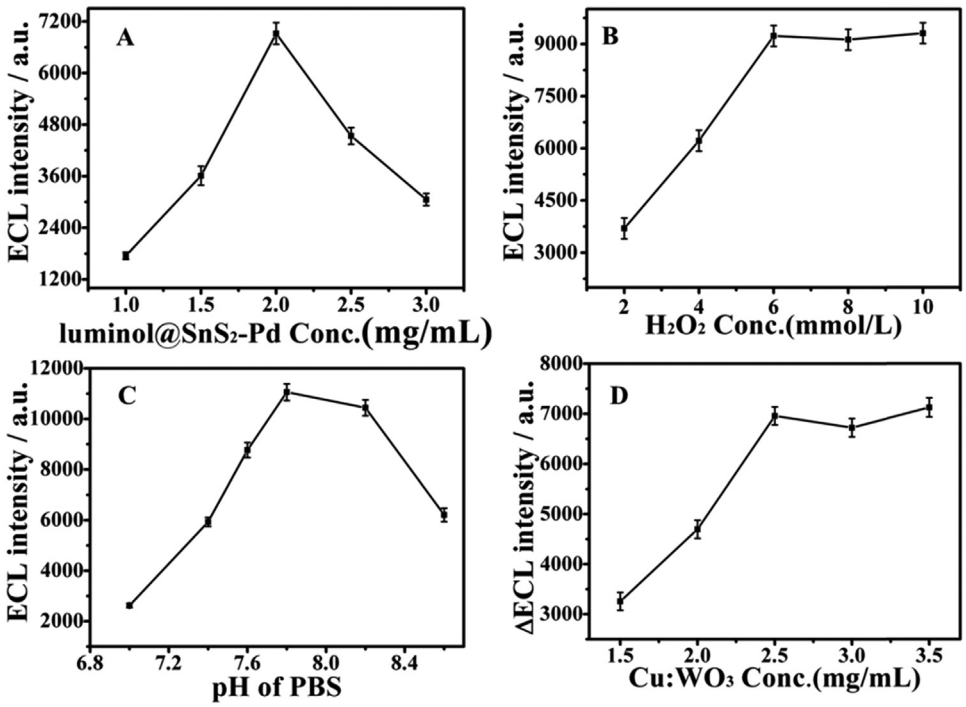

Fig. 2. The effect of concentration of luminol@SnS_2-Pd (A), concentration of H_2O_2 (B), the pH of PBS (C) on the response of ECL intensity from GCE/ luminol@SnS_2-Pd. (D) The effect of Cu: WO_3 concentrations on the ECL biosensor for detection 0.1 ng/mL $A\beta_{1-42}$ (ΔECL intensity was the difference between GCE/luminol@SnS_2-Pd-Ab_1 and GCE/luminol@SnS_2-Pd-Ab_1/ BSA/ $A\beta_{1-42}$/Cu:WO_3-Au-Ab_2). Error bars = SD (n = 3).

3.4. Quenching effect of Cu:WO_3 towards luminol@SnS_2-Pd

The mechanism of Cu:WO_3 towards luminol-H_2O_2 system was investigated using luminol@SnS_2-Pd as donor and Cu:WO_3 as acceptor. Fine overlaps was found between the ECL emission of luminol@SnS_2-Pd and UV-vis spectroscopy of Cu:WO_3 (Fig. 3B). In order to further prove the quenching effect of immunosensor caused by copper doping, the UV-vis absorption spectra of Cu:WO_3 (a) and pure WO_3 (b) were compared (Fig. S5). Compared curve a with b, the UV-vis absorption peaks showed red shift, and the absorption peaks become wider, which

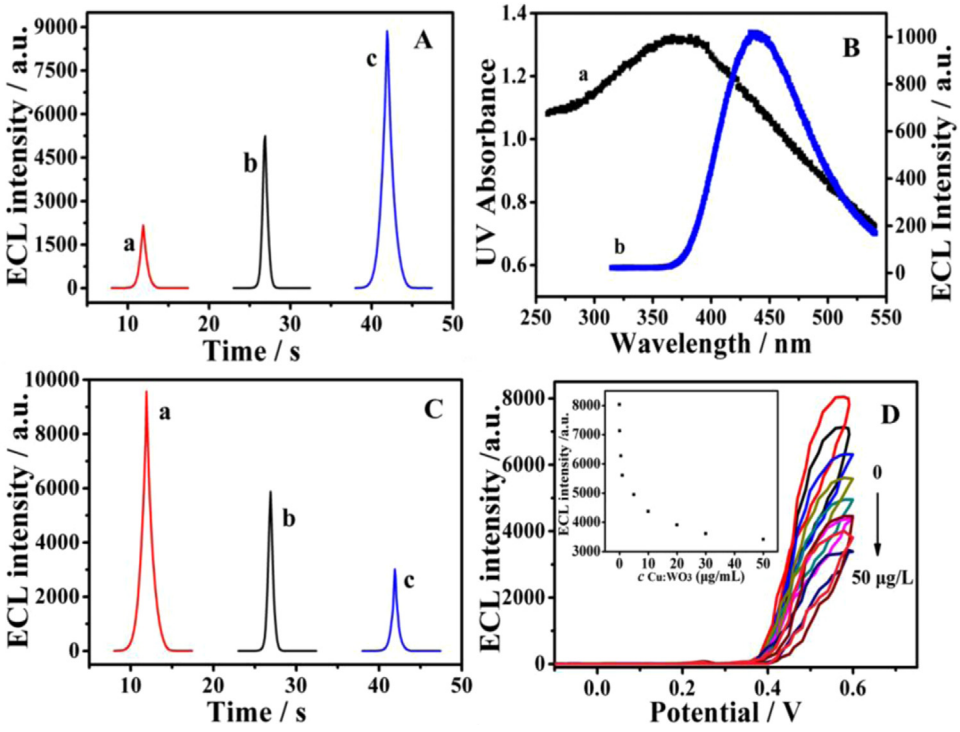

Fig. 3. (A) ECL behavior of bare GCE (a), SnS_2 nanoflowers (b), SnS_2-Pd composite (c), (B) ECL spectra of luminol@SnS_2-Pd (a), UV-vis absorption spectra of Cu: WO_3 (b), (C) ECL behavior of the (a) GCE/luminol@SnS_2-Pd, (b) GCE/luminol@SnS_2/WO_3-Au, (c) GCE/luminol@SnS_2/Cu:WO_3-Au in PBS (pH 7.8) containing 7 mM H_2O_2, (D) ECL of luminol@SnS_2-Pd in the presence of 0, 0.1, 0.5, 1, 5, 10 and 50 μg/L Cu:WO_3-Au (top to bottom). Inset: dependence of ECL intensity on Cu:WO_3-Au concentration.

lay a foundation for the increase of effective spectrum overlap and effective quenching. Layers of GCE/luminol@SnS_2-Pd-Ab_1/BSA/$A\beta_{1-42}$ electrodes were used as the initial ECL probes (curve a). Then, WO_3 (curve b) and Cu: WO_3 (curve c) was further modified on the above prepared electrode, respectively. As shown in Fig. 3C, the quenching effect of Cu:WO_3 was better than that of pure WO_3. In order to test the quenching effect, the ECL quenching of luminol@SnS_2-Pd was explored at GCE in 10 mL PBS (pH 7.8) containing 6 mM H_2O_2 and different concentrations of Cu:WO_3 (Fig. 3D). With the increase of Cu:WO_3 concentration, the ECL peak intensity decreased (inset in Fig. 3D). Based on existing work (Feng et al., 2015), the plot of I_0/I versus the concentration of Cu:WO_3 was made (Fig. S6), and it gave a detectable range of Cu:WO_3 from 0.05 to 10 μg/L (R^2 = 0.997, n = 7), which indicated a quenching mechanism described by the Stern-Volmer equation. Here I_0 and I were the ECL intensity in the absence and presence of quencher, respectively. From the plot, the quenching constant K_{sv} was found to be 2.8×10^5 g^{-1}. The large value of K_{sv} proved the good quenching effect of Cu:WO_3.

3.5. Characterization of the immunosensor

In order to prove the success of this immunosensor construction, the ECL responses of different nanocomposites used as the ECL probes were shown in Fig. 4A, which were carried out in PBS (pH 7.8) containing 6 mM H_2O_2. The bare GCE produced a weak ECL (curve a) and when the bare GCE was modified with luminol@SnS_2-Pd, the ECL responses were generated (curve b). It was clear that SnS_2-Pd could be combined with luminol through the electrostatic adsorption, indicating the excellent ECL nature of luminol and the favorable supporting ability and catalytic properties of the SnS_2-Pd composite (Zhang et al., 2018). After modification step by step (curve c-e), the electron transfer became more and more difficult, which made the impedance values increase gradually. When the Cu:WO_3-Au-Ab_2 was decorated on the electrode (curve f), the electron transfer resistance obviously increased, which reduced the ECL signal in turn.

Electrochemical impedance spectroscopy was performed at different modified-electrodes in 2.5 mM $[Fe(CN)_6]^{3-/4-}$ and 0.1 M KCl. EIS curves of the GCE at different modification steps were shown in Fig. 4B. The bare GCE exhibited a small semicircle domain (curve a), which indicated the mass-transfer process (Shu et al., 2017). When luminol@SnS_2-Pd was modified on the electrode surface, curve b showed a small semicircle but a little bigger than curve a, indicating that the electrochemical process would be subject to diffusion control and the material itself (Zou et al., 2017), which would result in a certain impedance

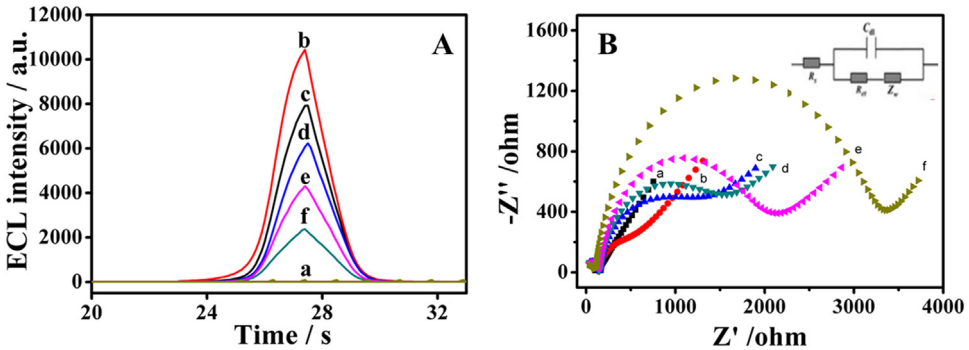

Fig. 4. ECL signal (A) and the corresponding EIS responses (B) of: (a) bare GCE, (b) GCE/ luminol@SnS_2-Pd, (c) GCE/luminol@SnS_2-Pd-Ab_1, (d) GCE/luminol@SnS_2-Pd-Ab_1/BSA, (e) GCE/luminol@SnS_2-Pd-Ab_1/BSA/$A\beta_{1-42}$, (f)GCE/luminol@SnS_2-Pd-Ab_1/BSA/$A\beta_{1-42}$/Cu: WO_3-Au-Ab_2.

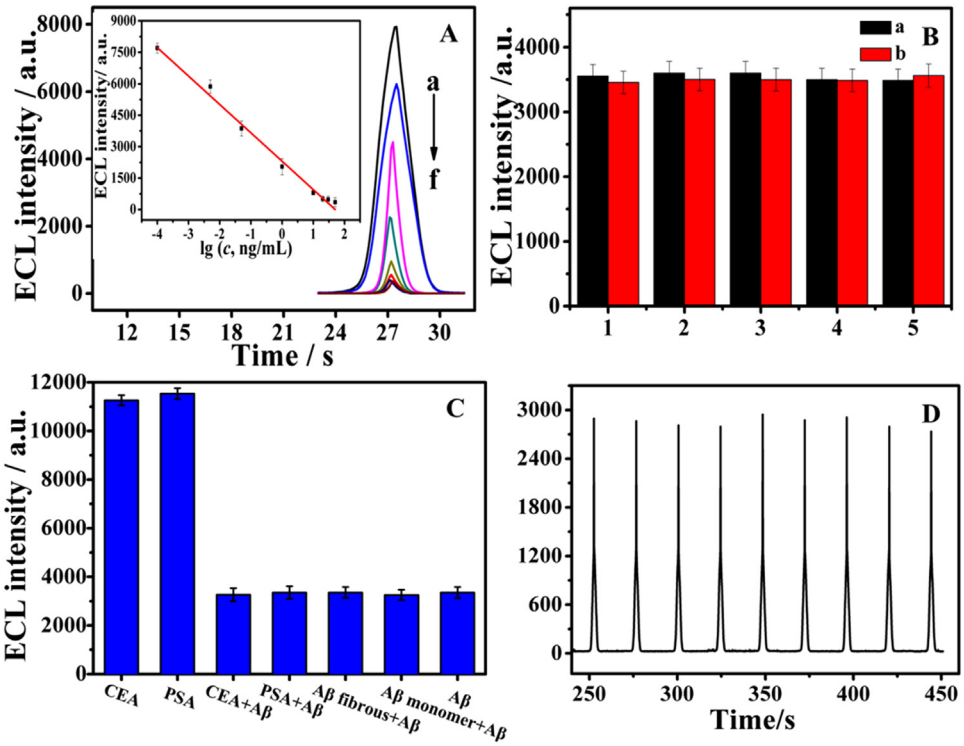

Fig. 5. (A) ECL response of the immunosensor to different concentrations of $A\beta_{1-42}$ (a-f): 0.0001, 0.001, 0.005, 0.05, 0.1, 5, and 50 ng/mL, and the corresponding calibration curve inset. All of the immunosensors were detected in 10 mL of PBS (pH 7.8) containing 6 mM of H_2O_2, (B) The reproducibility of the immunosensor for $A\beta_{1-42}$ was investigated with intra- (a) and interassay (b) precision, (C) The ECL intensity responses of the biosensors to separate 10 ng/mL CEA, PSA and 0.1 ng/mL $A\beta_{1-42}$ with 10 ng/mL interferences. Error bars = SD (n = 3), (D) Stability of the ECL immunosensor for 9 cycles.

effect. After the modification of Ab_1 (curve c), BSA (curve d) and $A\beta_{1-42}$ (curve e) layer by layer, the electron transfer also became more and more difficult and the impedance value increased gradually. In particular, when Cu:WO_3-Au-Ab_2 was modified, the electron transfer resistance increased significantly. Herein, the equivalent circuit element of the simulation parameter was used to simulate the circuit, so as to observe the impedance further (Table S1). The above results indicated the success of construction of the proposed immunosensor.

3.6. Analysis of $A\beta_{1-42}$

The effective ECL-RET between luminol@SnS_2-Pd and Cu:WO_3-Au was applied to sensitively detect a series of different concentrations of $A\beta_{1-42}$. The calibration curve was drawn in Fig. 5A, which ECL intensity I_{ECL} as vertical coordinate and log c as horizontal coordinate. Its linear regression equation was $I_{ECL} = 2306–1355 \times \lg c$, with the linear regression coefficient $R^2 = 0.9919$. The linear range was from 0.0001 ng/mL to 50 ng/mL, What's more, the detection limit of this system was 5.4 fg/mL (S/N = 3). To further illustrate the superiority of the method, there was comparing this work with other related work (Table S2). The results showed that the detection limit of the immunosensor was lower and the detection range was wider, which provide important guidance for the detection of $A\beta_{1-42}$ and other biomarkers.

3.7. Repeatability, stability and specificity of the immunosensor

The reproducibility, stability and specificity were investigated to detect the performance of the immunosensor (Sheng et al., 2018; Wu et al., 2018). The reproducibility of the immunosensor for $A\beta_{1-42}$ was investigated with intra- and interassay precision. The intra-assay precision was evaluated by testing one $A\beta_{1-42}$ level for five reduplicate measurements. The interassay precision was estimated by detecting one $A\beta_{1-42}$ level with five immunosensors. The intra- and interassay variation coefficients obtained from 0.1 ng/mL $A\beta_{1-42}$ are 2.4% and 2.7%, respectively, indicating good precision and reproducibility of the immunosensor (Fig. 5B).

To assess the specificity, ECL responses of the immunosensor towards CEA, PSA were investigated. As shown in Fig. 5C, the ECL response of the proposed immunosensor incubating with a mixture solution (0.1 ng/mL $A\beta_{1-42}$ containing 10 ng/mL CEA, 10 ng/mL PSA, 10 ng/mL $A\beta_{1-42}$ monomer and 10 ng/mL $A\beta_{1-42}$ fibrous, respectively) almost the same with that incubating with 0.1 ng/mL $A\beta_{1-42}$ and its RSD was below 1.42%. In addition, ECL responses of the immunosensor towards separate CEA and PSA (10 ng/mL) were investigated. All of results indicated the high specificity of the ECL immunosensor.

Operation stability is important for extending potential application in the immunosensor field (Huang et al., 2017). There displayed ECL emission of the immunosensor for detection of 0.1 ng/mL $A\beta_{1-42}$ under giving continuous potential to the working electrode 9 cycles. The immunosensor showed excellent stability with the RSD of 1.7%, which indicated that the sensing signal was reliable (Fig. 5D).

3.8. Application in human CSF sample

The recovery rate of different concentration of $A\beta_{1-42}$ in human CSF was determined by means of a standard recovery method (Table S3). The RSD was less than 3.6%. The recovery range was from 95.2% to 96.8%. F-test is conducted to determine the accuracy whether there is a significant difference. Based on the F-test, the calculated F value (Eq. (1)) is less than the theoretical one ($F = 6.39$ at 95% confidence limits), demonstrating the precisions of these two methods are highly equivalent. The results are shown in the Table S4. Meanwhile, ELISA kit was also conducted to evaluate the proposed immunosensor. The concentration of the CSF sample was tested five times by ELISA kit, respectively. T-test is also adopted to evaluate this sandwich strategy (Table S4). By t-test analysis (Eq. (2)), the mean values are not obviously different from the data gained from ELISA kit. The t value is less than 2.78 ($P = 0.95$, $\alpha = 0.05$, $f = 4$). The results show the system error can be ignored. Through the F-test and t-test, the precision and accuracy can be ensured.

$$F = \frac{S_{big}}{S_{little}} \quad (1)$$

$$t = \frac{|\bar{x}-\mu|}{s}\sqrt{n} \quad (2)$$

4. Conclusion

In conclusion, this work constructed an ECL-RET system utilizing luminol@SnS_2-Pd as a donor and Cu:WO_3 as an acceptor to realize sensitive detection of $A\beta_{1-42}$. In this experiment, SnS_2-Pd with excellent catalytic effect was prepared to combine with luminol to obtain a higher ECL signal, while mesoporous Cu:WO_3 was used to quench the ECL signal due to ECL-RET between SnS_2-Pd-luminol and Cu:WO_3. This strategy showed sensitive response to $A\beta_{1-42}$ concentration from 0.1 pg/mL to 50 ng/mL with a low detection limit of 5.4 fg/mL (S/N = 3). The immunosensor showed good selectivity, stability and reproducibility. It could be applied to detect other biomarkers and find potential tools for early diagnose of some diseases.

CRediT authorship contribution statement

Jingwei Xue: Data curation, Investigation, Visualization, Writing - original draft. **Lei Yang:** Conceptualization, Formal analysis, Methodology. **Huan Wang:** Conceptualization, Formal analysis, Methodology. **Tao Yan:** Supervision, Writing - review & editing. **Dawei Fan:** Supervision, Writing - review & editing. **Rui Feng:** Supervision, Writing - review & editing. **Bin Du:** Project administration, Resources. **Qin Wei:** Project administration, Resources. **Huangxian Ju:** Project administration, Resources.

Acknowledgements

This study was supported by the Natural Science Foundation of Shandong Province, China (No. ZR2017BB030), National Key Scientific Instrument and Equipment Development Project of China (No. 21627809), National Natural Science Foundation of China (Nos. 21575050, 21777056, 21505051).

Author contributions

J.W. X., L. Y., H. W. conceived and designed the experiments. J.W. X. performed the experiments, analyzed the data and wrote the first draft of the manuscript. T. Y., D.W. F., R. F., B. D., Q. W., and H.X. J. contributed substantially to revisions. All the authors discussed the results and commented on the manuscript.

Declaration of interests

None.

Appendix A. Supporting information

Supplementary data associated with this article can be found in the online version at doi:10.1016/j.bios.2019.03.035.

References

Afsharmohajer, N., Zuidema, C., Sousan, S., Hallett, L., Tatum, M., Rule, A.M., Thomas, G., Peters, T., Koehler, K., 2018. J. Occup. Environ. Hyg. 15 (2), 87–98.
Ahmed, B., Anjum, D.H., Hedhili, M.N., Gogotsi, Y., Alshareef, H.N., 2016. Nanoscale 8 (14), 7580–7587.
Ahmed, M.U., Lim, S.A., 2016. RSC Adv. 6 (30), 24995–25014.
Ahmed, M.U., Saaem, I., Wu, P.C., Brown, A.S., 2014. Crit. Rev. Biotechnol. 34 (2), 180–196.
Cao, Y., Yuan, R., Chai, Y., Mao, L., Niu, H., Liu, H., Zhuo, Y., 2012. Biosens. Bioelectron. 31 (1), 305–309.
Chang, K., Wang, Z., Huang, G., Li, H., Chen, W., Lee, J.Y., 2012. J. Power Sources 201, 259–266.
Chianelli, R.R., Daage, M., Ledoux, M.J., 1994. Adv. Catal. 40, 177–232.
Deng, X., Wang, C., Shao, M., Xu, X., Huang, J., 2017. RSC Adv. 7 (8), 4329–4338.
Feng, Y., Dai, C., Lei, J., Ju, H., Cheng, Y., 2015. Anal. Chem. 88 (1), 845–850.
Feng, Y., Sun, F., Wang, N., Lei, J., Ju, H., 2017. Anal. Chem. 89 (14), 7659–7666.
Frens, G., 1973. Nat. Phys. Sci. 241 (105), 20–22.
Fu, X., Zhou, L., 2011. J. Inorg. Organomet. P. 21 (4), 958–961.
Ghedini, E., Menegazzo, F., Signoretto, M., Manzoli, M., Pinna, F., Strukul, G., 2010. J. Catal. 273 (2), 266–273.
Hu, J.H., Mi, H., Wang, N., Zhu, H.Y., Guo, W.Y., Zhang, S.R., Shi, F., Lei, Z.B., Liu, Z.H., Jiang, R.B., 2018. Nanoscale 10 (12), 5607–5616.
Huang, Z.J., Han, W.D., Wu, Y.H., Hu, X.G., Yuan, Y.N., Chen, W., Peng, H.P., Liu, A.L., Lin, X.H., 2017. J. Electroanal. Chem. 785, 8–13.
Jia, Y., Yang, L., Feng, R., Ma, H., Fan, D., Yan, T., Feng, R., Du, B., Wei, Q., 2019. ACS Appl. Mater. Interfaces 11 (7), 7157–7163.
Jin, H., Huynh, T.P., Haick, H., 2016. Nano Lett. 16 (7), 4194–4202.
Jin, T., Wan, J., Dai, C., Qu, S., Shao, J., Ma, F., 2018. J. Appl. Electrochem. 48 (3), 1–11.
Jing, L., Xu, Y., Zhang, M., Xie, M., Xu, H., He, M., Liu, J., Huang, S., Li, H., 2017. Inorg. Chem. Front. 5 (4), 63–72.
Kadimisetty, K., Malla, S., Sardesai, N.P., Joshi, A.A., Faria, R.C., Lee, N.H., Rusling, J.F., 2015. Anal. Chem. 87 (8), 4472–4478.
Liu, H., Crooks, R.M., 2012. Anal. Chem. 84 (5), 2528–2532.
Long, X., Zhang, F., He, Y., Hou, S., Zhang, B., Zou, G., 2018. Anal. Chem. 90 (5), 3563–3569.
Lu, Y., Yuan, M., Liu, Y., Tu, B., Xu, C., Liu, B., Zhao, D., Kong, J., 2005. Langmuir 21 (9), 4071–4076.
Ma, H., Zhao, Y., Liu, Y., Zhang, Y., Wu, D., Li, H., Wei, Q., 2017. Anal. Chem. 89 (24), 13049–13053.
Ren, K., Xu, Y., Liu, Y., Yang, M., Ju, H., 2017a. ACS Nano 12 (1), 263–271.
Ren, X., Ma, H., Zhang, T., Zhang, Y., Yan, T., Du, B., Wei, Q., 2017a. ACS Appl. Mater. Interfaces 9 (43), 37637–37644.
Ren, X., Yan, J., Wu, D., Wei, Q., Wan, Y., 2017b. ACS Sens. 2 (9), 1267–1271.
Rizwan, M., Mohd-Naim, N.F., Ahmed, M.U., 2018. Sensors 18 (2), 166–193.
Sheng, J., Jiang, X., Wang, L., Yang, M., Liu, Y.N., 2018. Anal. Chem. 90 (4), 2926–2932.
Shi, W., Feng, G., Wang, H., Guo, S., Hao, L., Zhou, Y., Cheng, Z., Liu, Y., Hui, H., Mao, B., 2017. ACS Appl. Mater. Interfaces 9 (24), 20585–20593.
Shu, J., Han, Z., Zheng, T., Du, D., Zou, G., Cui, H., 2017. Anal. Chem. 89 (23), 12636–12640.
Sloan, J.H., Siegel, R.W., Ivanova-Cox, Y.T., Watson, D.E., Deeg, M.A., Konrad, R.J., 2012. Clin. Biochem. 45 (18), 1640–1644.
Sperling, R.A., Aisen, P.S., Beckett, L.A., Bennett, D.A., Craft, S., Fagan, A.M., Iwatsubo, T., Clifford, R., Jack, J., Kaye, J., Montine, T.J., 2011. Alzheimers Dement. 7 (3), 280–292.
Warczak, M., Gryszel, M., Jakešová, M., Đerek, V., Głowacki, E.D., 2018. Chem. Commun. 54 (16), 1960–1963.
Wu, D., Wei, Y., Ren, X., Ji, X., Liu, Y., Guo, X., Liu, Z., Asiri, A.M., Wei, Q., Sun, X., 2018. Adv. Mater. 30 (9), 1705366–1705372.
Xiang, Q., Meng, G.F., Zhao, H.B., Zhang, Y., Li, H., Ma, W.J., Xu, J.Q., 2013. J. Phys. Chem. C. 114 (5), 2049–2055.
Xiang, R., Dan, W., Ge, R., Xu, S., Ma, H., Tao, Y., Yong, Z., Du, B., Qin, W., Liang, C., 2018. Nano Res. 11, 2024–2033.
Xing, B., Zhu, W., Zheng, X., Zhu, Y., Qin, W., Dan, W., 2018. Sens. Actuators B Chem. 265, 403–411.
Yang, L., Li, Y., Zhang, Y., Fan, D., Pang, X., Wei, Q., Du, B., 2017a. ACS Appl. Mater. Interfaces 9 (40), 7157–7163.
Yang, L., Zhu, W., Ren, X., Khan, M.S., Zhang, Y., Du, B., Wei, Q., 2017b. Biosens. Bioelectron. 91, 842–848.
Yang, Y., Yang, Z., Lv, J., Yuan, R., Chai, Y., 2017c. Talanta 169, 44–49.
Zhang, R., Adsetts, J.R., Nie, Y., Sun, X., Ding, Z., 2018. Carbon 129, 45–53.
Zhou, T., Pang, W.K., Zhang, C., Yang, J., Chen, Z., Liu, H.K., Guo, Z., 2014. ACS Nano 8 (8), 8323–8333.
Zou, G., Tan, X., Zhang, B., Zhou, J., 2017. Chem. Electro Chem. 4 (7), 1714–1718.